



Microscopic brain tumor detection and classification using 3D CNN and feature selection architecture

Amjad Rehman¹ | Muhammad Attique Khan² | Tanzila Saba¹ | Zahid Mehmood³ | Usman Tariq⁴ | Noor Ayesha⁵

¹Artificial Intelligence & Data Analytics Lab CCIS, Prince Sultan University, Riyadh, Saudi Arabia

²Department of Computer Science, HITEC University, Taxila, Pakistan

³Department of Computer Engineering, University of Engineering and Technology, Taxila, Pakistan

⁴College of Computer Engineering and Science, Prince Sattam bin Abdulaziz University, Saudi Arabia

⁵School of Clinical Medicine, Zhengzhou University, Zhengzhou, China

Correspondence

Amjad Rehman, Artificial Intelligence & Data Analytics Lab CCIS, Prince Sultan University, Riyadh, Saudi Arabia.
Email: rkamjad@gmail.com

Funding information

Prince Sultan University Riyadh Saudi Arabia,
Grant/Award Number: SEED-CCIS-2020(30)

Review Editor: Peter Saggau

Abstract

Brain tumor is one of the most dreadful natures of cancer and caused a huge number of deaths among kids and adults from the past few years. According to WHO standard, the 700,000 humans are being with a brain tumor and around 86,000 are diagnosed since 2019. While the total number of deaths due to brain tumors is 16,830 since 2019 and the average survival rate is 35%. Therefore, automated techniques are needed to grade brain tumors precisely from MRI scans. In this work, a new deep learning-based method is proposed for microscopic brain tumor detection and tumor type classification. A 3D convolutional neural network (CNN) architecture is designed at the first step to extract brain tumor and extracted tumors are passed to a pre-trained CNN model for feature extraction. The extracted features are transferred to the correlation-based selection method and as the output, the best features are selected. These selected features are validated through feed-forward neural network for final classification. Three BraTS datasets 2015, 2017, and 2018 are utilized for experiments, validation, and accomplished an accuracy of 98.32, 96.97, and 92.67%, respectively. A comparison with existing techniques shows the proposed design yields comparable accuracy.

KEY WORDS

3D CNN, cancer, healthcare, public health, World Health Organization (WHO)

1 | INTRODUCTION

Among numerous cancer types, a brain tumor is one the most dreadful nature of cancer and caused a massive number of deaths among kids and adults (Iqbal, Khan, Saba, & Rehman, 2017; Saba, Mohamed, El-Affendi, Amin, & Sharif, 2020). The latest World Health Organization (WHO) survey stated that 700,000 humans are being with a brain tumor and around 86,000 are diagnosed since 2019. From 700,000, 69.1% of persons are diagnosed by a benign tumor while 30.1% are malignant. However, the approximated number of deaths due to brain tumor is 16,830 since 2019 and the average survival rate is 35% (NBTC, 2019). Due to the considerable number of deaths, nowadays, it is the hottest research topic in medical imaging (Mittal et al., 2020; Rehman et al., 2020). However, the early identification of tumors

could increase the human survival rate by a malignant tumor (Khan et al., 2020). The tumor is treated under specific grades such as Grade 1 to Grade 4. The Grade 1 tumor called benign while the Grade 4 tumor described as malignant (WHO standard).

For the treatment of tumors, physicians use several options such as chemotherapy, radiotherapy, and surgery, however; it always depends on the size, shape, and nature of a tumor (Ejaz et al., 2018; Rehman et al., 2020). The clinical technology like MRI yields detailed information of healthy and tumor regions in the forms of their slices (Amin et al., 2019; Amin, Sharif, Yasmin, & Raza, 2019; Ramzan, Khan, Iqbal, Saba, & Rehman, 2020; Tahir et al., 2019). However, due to many slices, it is still a challenging problem to check the tumor abnormality. The clinical experts analyze these slices one by one which is a time-consuming and challenging process (Grade et al., 2015).

Moreover, with a human naked eye, it is not possible to diagnose a tumor in all slices. Hence, an expert radiologist is required for accurate identification of a brain tumor. Therefore, the automated systems are always required to diagnose a tumor in the MR images without human intervention.

Currently, in the state of art, various computerized techniques are proposed by computer vision researchers for brain tumor classification using MRI. They mostly focused on four types of brain tumor categories such as T1, T1 CE, T2, and Flair as shown in Figure 1. In this figure, it is illustrated that the Flair and T1CE tumors are more visible as compared to T2 and T1.

Further, in Figure 2, a few benign and malignant scans are also illustrated that describe another critical challenge for accurate classification. The comprehensive computerized techniques reported in state of art mostly follow well-known steps such as tumor detection using segmentation techniques (e.g., K-Means Nanda, Gulati, Chauhan, Modi, & Dhaked, 2019), Watershed methodology (Khan et al., 2019), Saliency-based distinctive features extraction (e.g., shape, geometric, region props, wavelet, etc.; Banerjee, Mitra, & Shankar, 2018; Arunkumar et al., 2020), and finally classification using machine learning algorithms (SVM, KNN, NN, etc.; Sharif, Li, Khan, & Saleem, 2020). However, these techniques are not performed well when the MRI scans have low contrast and the features are not relevant to the enigma report. Further, these techniques work on very limited data and accuracy demoted for data exceeded a specific limit. To handle this problem, lately, a deep learning scheme is proposed by machine learning experts and provides a handsome accuracy for all computer vision applications like skin cancer (Javed, Rahim, & Saba, 2019; Javed, Rahim, Saba, & Rashid, 2019; Saba, Khan, Rehman, & Marie-Sainte, 2019), agriculture (Khan et al., 2018), breast cancer (Mughal, Muhammad, Sharif, Rehman, & Saba, 2018; Mughal, Muhammad, Sharif, Saba, & Rehman, 2017; Saba et al., 2019), blood cancer (Abbas et al., 2018; Abbas et al., 2019; Rehman, Abbas, Saba, Mahmood, & Kolivand, 2018; Rehman et al., 2018), lungs cancer (Saba, Sameh, Khan, Shad, & Sharif, 2019), and several other human body diseases (Al-Ameen et al., 2015; Fahad, Khan, Saba, Rehman, & Iqbal, 2018; Husham, Alkawaz, Saba, Rehman, & Alghamdi, 2016; Iftikhar, Fatima, Rehman, Almazyad, & Saba, 2017; Jamal, Hazim Alkawaz, Rehman, & Saba, 2017; Nodehi et al., 2014; Norouzi et al., 2014; Perveen et al., 2020; Rahim, Norouzi, Rehman, & Saba, 2017; Rahim, Rehman, Kurniawan, & Saba, 2017; Ramzan

et al., 2020; Saba, 2017; Saba, Bokhari, Sharif, Yasmin, & Raza, 2018; Saba, Rehman, Mehmood, Kolivand, & Sharif, 2018; Ullah et al., 2019; Yousaf et al., 2019). In usual, a simple deep learning model consists of a series of layers such as convolution that process the input image into several patches, ReLu activation function, Pooling layer for features reduction, and FC layer. The FC layer is most important in the convolutional neural network (CNN) that extracts the highly related and depth-based features of a specific problem like various tumor types classification.

It has been observed that deep learning strategies for brain tumor classification achieved better results than traditional techniques (Jadooki, Mohamad, Saba, Almazyad, & Rehman, 2017; Khan et al., 2020). Therefore, in this article, we consider the problem of inaccurate segmentation of the brain tumor and robust convolutional neural features for classification. For this purpose, a new fully automated 3D CNN-based model is proposed that segment the tumor at the very first stage and further classify it into their relevant categories such as T1, T2, T1CE, and Flair.

In the previously automated methods (Khan, Lali, et al., 2019; Padlia & Sharma, 2019; Saba, Mohamed, et al., 2020), the authors performed the preprocessing step to enhance the region of interest (ROI) which improves the detection accuracy followed by conventional methods like K-means, GrabCut, watershed, and many more. The conventional methods did not work well without preprocessing steps and demoted the detection performance. Further, the selection of most discriminant points is essential to extract for correct tumor classification according to its type. Therefore, in this work, a 3D CNN-based architecture is proposed for accurate tumor detection with a higher precision rate. The further correlation-based method along with feed-forward neural (FNN) is also proposed for correct tumor type classification.

Further paper is organized in four sections, Section 2 explores related work, Section 3 presents the proposed methodology, Section 4 exhibits experimental results and analysis, Section 5 concludes the research along with future work.

2 | RELATED WORK

The brain is an important organ of the human nervous system. For the diagnosis of brain tumor, MRI is mostly used in hospitals (Nodehi

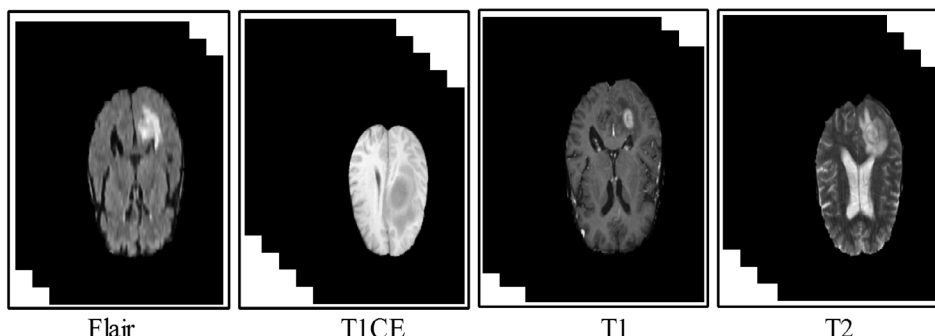


FIGURE 1 Categories of brain tumor

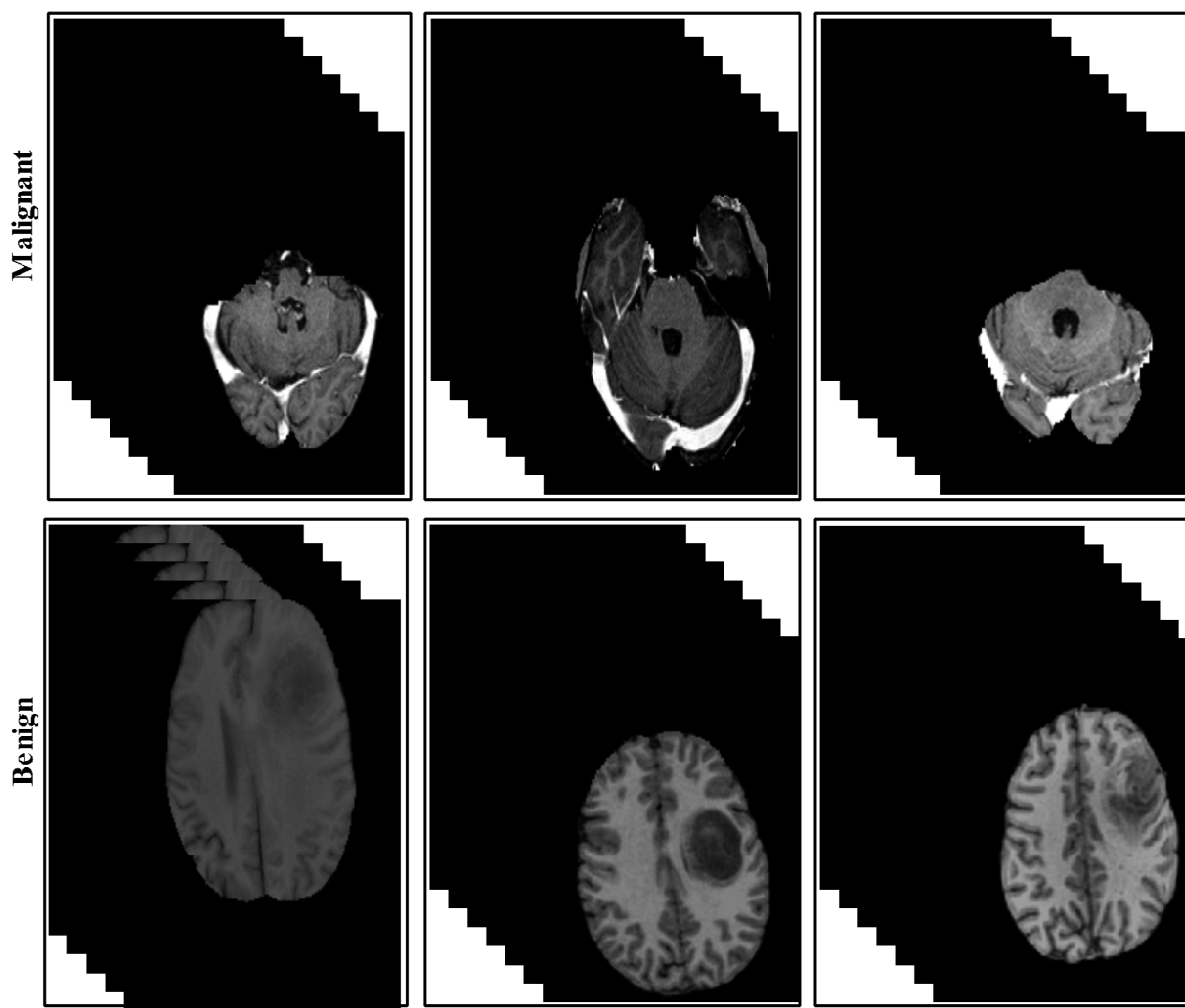


FIGURE 2 Representation of benign and malignant tumors

et al., 2014). Several semiautomated and fully automated techniques are presented in the literature for brain tumor detection and classification. The deep learning is the emerging technology in machine learning and has attracted significant attention in medical image processing especially for brain tumor detection (Iqbal, Ghani, Saba, & Rehman, 2018; Khan et al., 2020). Additionally, in the area of medical image processing, machine learning has attracted high attention and comes out with notable performance for tumor detection for various modalities such as dermoscopy (Afza, Khan, Sharif, & Rehman, 2019; Javed, Rahim, Saba, & Rehman, 2020), MRI (Nazir, Khan, Saba, & Rehman, 2019;), Mammography (Marie-Sainte, Saba, Alsaleh, Alotaibi, & Bin, 2019; Saba, Khan, Islam, et al., 2019), and so on.

Saba, Mohamed, et al. (2020) used GrabCut strategy to extract texture features from MRI for brain tumor classification. With VGG-19 (CNN architecture) 98.78, 99.63, and 99.67% accuracy reported on (BraTS) 2015, 2016, and 2017, respectively. Ejaz et al. (2020) proposed hybrid SOM pixel labeling with reduce cluster membership and deterministic feature clustering for brain tumor identification using MICCAI BraTS dataset. To segment brain tumor, cluster obtained

using three unsupervised learning techniques. They tested method using dice overlap index, Jaccard Tanimoto coefficient index, mean squared error, and peak signal to noise ratio. The obtained results were 98%, 96%, 0.06, 18 lb, respectively.

Arunkumar et al. (2020) presented an automated model-based segmentation and ANN-based tumor classification using MRI scans. In their approach, ROI is extracted using model-based segmentation which later utilized for textural descriptors. The extracted textural descriptors are recognized through ANN and achieved enhanced performance for 200 MRI cases. Sharif et al. (2020) introduced a feature selection approach that selects the best CNN features for classification. In their approach, the contrast of original MRI images is improved and implemented a saliency-based approach for tumor detection. Later, the inception CNN model is used with the help of TL to extract the deep features. Additionally, the DRLBP features are also concatenated with CNN features and the best of them are selected using the PSO method. The experiments performed on the BraTS dataset series and attained refined accuracy. Khan et al. (2020) proposed multimodal automatic brain tumor classification strategy using

deep learning. Linear contrast stretching, transfer learning-based features extraction using pretrained CNN models (VGG16 & VGG19), features selection based on correntropy. Robust covariant features centered on the partial least square fused in one matrix. Finally, fused matrix fed to the extreme learning mechanism (ELM) to classify brain tumor. The proposed approach validated on the BraTS datasets and achieved an accuracy of 97.8, 96.9, 92.5%, respectively, for BraTs2015, BraTs2017, and BraTs2018.

Sajjad et al. (2019) described a deep neural network (DNN) based design for the detection of multigraded brain tumors in the MRI images. The extracted tumors using deep learning are further increased by data augmentation and used a pretrained CNN for training on newly captured segmented images. Later on, the validation is performed on both augmented and original stored datasets and notes a significant change in the accuracy. Sajid, Hussain, and Sarwar (2019) introduced a deep learning model for different brain modalities segmentation. They use MRI datasets for this task and trained the hybrid CNN model for the extraction of the local and contextual knowledge of tumors. Thereafter, the overfitting problem is solved and passed to feed-forward NN for training. Overall, the presented approach produced a better precision rate on selected BraTS series during the validation.

Iqbal et al. (2019) proposed a deep learning model for brain tumor segmentation by merging short-term memory (LSTM) and coevolutionary neural networks (ConvNet) concepts. Following preprocessing,

to address the class inequality issues, the class-weighting concept is introduced. BraTS 2018 benchmark dataset employed for experiments and ConvNet as a single score (exactitude) of 75% while 80% is produced by an LSTM-based network, with a total fusion of 82.29% accuracy.

The aforementioned studies focus on patch-based method and use traditional techniques for segmentation like GrabCut, Gabor, K-Means, and so on. However, these techniques are unsuitable for a significantly large number of MRI database for brain tumor detection. Therefore, it is essential to implement a precise, efficient, and consistent method for tumor detection and classification from MR images using enhanced deep learning techniques.

3 | PROPOSED METHODOLOGY

A new 3D CNN and correlation along FNN based automated approach is proposed in this work for brain tumor detection and classification. The proposed method consists of three core steps—(a) new CNN architecture based brain tumor extraction, (b) pretrained VGG19 based deep features extraction, and (c) Pearson correlation along with FNN features selection for final classification. A detailed architecture proposed scheme is illustrated in Figure 3. In this figure, it could be seen that the extracted tumor region is utilized for the next steps for precise tumor classification.

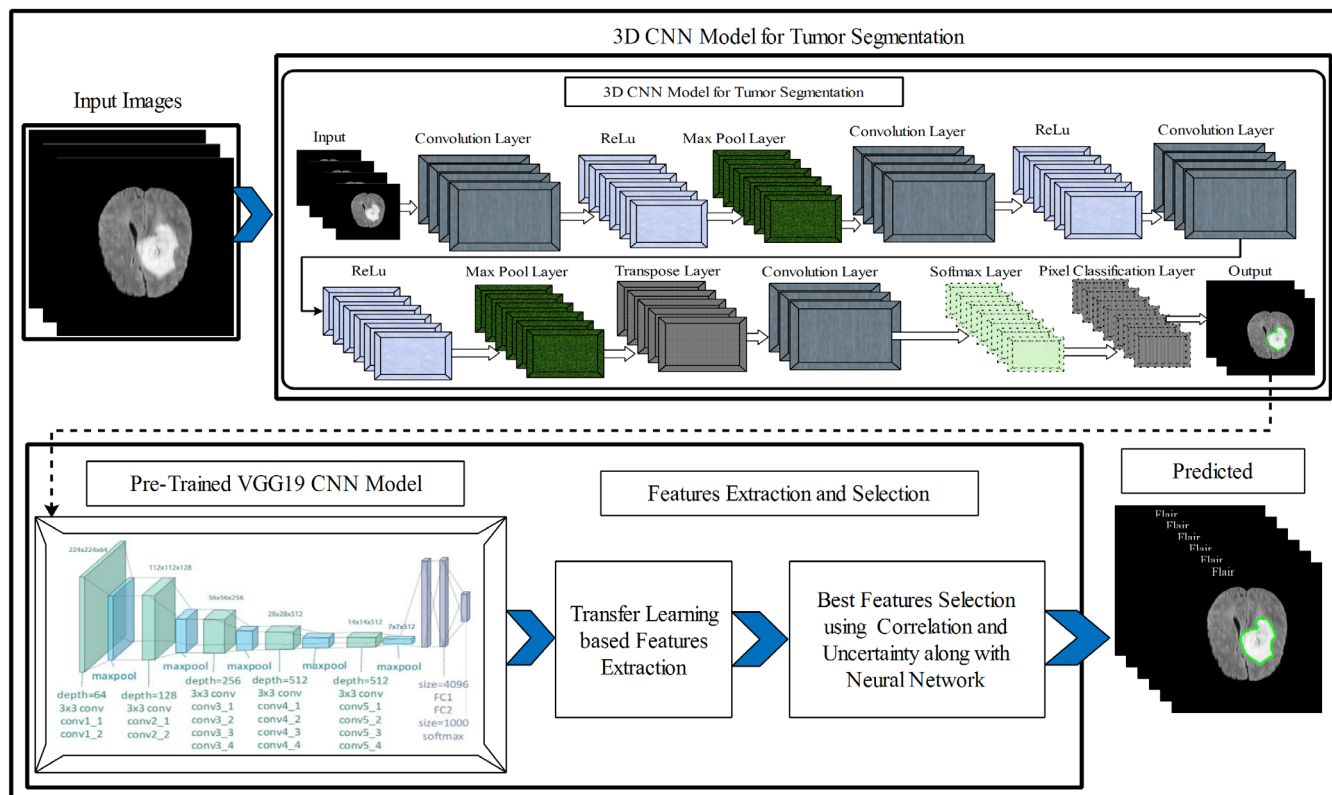


FIGURE 3 Proposed 3D CNN and feature selection design for tumor detection and classification [Color figure can be viewed at wileyonlinelibrary.com]

3.1 | BraTS Datasets

Three datasets are utilized in this work for training and validation of proposed architecture. The selected datasets are BraTS 2015, BraTS 2017, and BraTS 2018, respectively. Each database includes four different classes such as Flair, T1CE, T1, and T2 along with their ground-truth images. These datasets include both HGG and LGG type images. The selected ratio of both HGG and LGG patient cases in this work is depicted in Table 1. The resolutions of all images are anisotropic which resampled to isotropic. From this figure, the 60% flair and T1CE images along with their ground-truth images are employed to train a CNN model for the segmentation process. While the remaining 40% images and of these both classes and 100% of T1 and T2 are utilized for the testing process. The configuration and learning process of CNN model is detailed in the next sections.

3.2 | 3D CNN segmentation model

In this section, a 3D CNN-based architecture design for brain tumor classification is presented. As mentioned in the previous section, the reported techniques focused on a preprocessing step for better visualization of tumor pixels, however, in the CNN models, the rich features are computed from low-dose MRI scans. These rich features provide sufficient information on tumor region extraction. The proposed 3D CNN architecture deals with natural three-dimensional images for features calculation, whereas the input is passed to the next layers in the form of several patches. In Figure 4, a proposed 3D CNN architecture is presented. The mathematical detail of this model is given below.

Let us have an input image $\xi(x, y)$ of dimension $N \times M \times R$ where $M = 512$, $N = 512$, and $R = 3$, respectively. The notation N denotes row pixel values, M denotes column pixel values, and R represents the number of channels that are 3 in this work. Consider λ denote one patch of dimension $32 \times 32 \times 3$ and B represents i th patches, respectively, then convolution layer can be defined as:

$$\lambda_i^c = f \left(\sum_{m=1}^{\varphi_{i-1}} \psi_i^{m,n} \times \lambda_{i-1}^c + \beta_i^c \right) \quad (1)$$

where λ_{i-1}^c denotes the previous layer, λ_i^c denotes current layer, $\psi_i^{m,n}$ represents weights matrix, and β_i^c is a bias value for each patch,

TABLE 1 BraTS datasets for training and validation process

Dataset	Description
BraTS 2015	Total sets 274 including 192 training cases (154 HGG and 38 LGG) and 82 testing cases (66 HGG and 16 LGG)
BraTS 2017	Total sets 431 including 285 training cases (210 HGG and 75 LGG) and 146 testing cases for both HGG and LGG
BraTS 2018	Total sets 476 including 285 training cases (210 HGG and 75 LGG) and 191 testing cases for both HGG and LGG

respectively. The weights matrixes $\psi_i^{m,n}$ in each hidden layer are learned and return a 4D kernel matrix. These kernels can be concatenated in 4D as:

$$\left(\lambda_i^{m,1}, \lambda_i^{m,2}, \dots, \lambda_i^{m,\varphi_{i-1}} \right) \quad (2)$$

$$\lambda_{i-1} = \lambda_{i-1}^1, \lambda_{i-1}^2, \dots, \lambda_{i-1}^{\varphi_{i-1}} \quad (3)$$

This expression returns a more complex pattern of an image that later utilized for better identification of pixels nature. A ReLu activation function is utilized after the convolution layer for quick training. This function returns identity for all positive values while zero for all negative features. Further, this function can help to remove the problem of overfitting, mathematically, it is represented in Equation (4)

$$Y = \max(0, \lambda) \quad (4)$$

Further, a max-pooling operation is also performed for down sampling in CNN layers. As shown in Figure 4, two max-pooling layers are added in the proposed design to reduce the dimensionality of features. An example of max pooling is shown in Figure 5 where stride and pooling size of [2 2]. Later on, a transpose layer is added for upsampling. As we know about several interpolation techniques such as the nearest neighbor, bi-linear, and bi-cubic that are used for upsampling but in transposed convolution layer, these techniques are not performed. This layer includes several learnable parameters that help in the construction of the new resultant image. In this work, this layer classifies the pixels based on their labels that are defined at the earlier step. Finally, the pixel label classification layer is added that segment the tumor based on cross-entropy function as depicted in Equation (5):

$$\phi(\lambda, C) = -\frac{1}{B} \sum_{i=1}^B \log(p_C) \quad (5)$$

where λ , C denotes original patches of dimension $32 \times 32 \times 3$ and corresponding correct labels, B represents i th patches of one image, and p_C denotes the posterior probability for true class C .

3.3 | Training details

As presented in Table 2, the number of layers and their description is added. In this table, it is explained that a $32 \times 32 \times 3$ patch assumed as an input with zero center normalization. Then first convolution layer is added of stride [1 1] and padding [1 1 1]. Further, 2×2 max-pooling layer is opted of stride [1 1] and padding [0 0 0 0]. In the second pooling layer, stride is [2 2] and padding [0 0 0 0]. Following the initialization of all these layers, presented in Table 2, the neural network is trained. For training a neural network, the following parameters are initialized such as sigmoidal activation function, mini-batch size of 64, the learning rate of 0.001, the number of epochs is

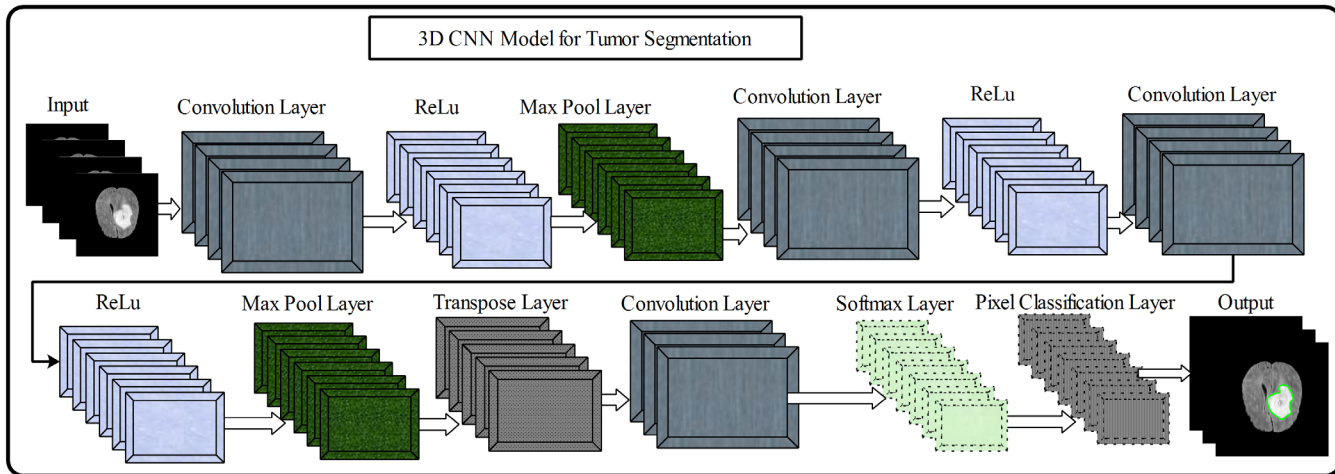


FIGURE 4 Proposed 3D CNN architecture for brain tumor extraction [Color figure can be viewed at wileyonlinelibrary.com]

0.785	0.467	0.954	0.473
0.744	0.554	0.628	0.342
0.884	0.776	0.732	0.114
0.555	0.824	0.825	0.995

→

0.785	0.954
0.884	0.995

FIGURE 5 An example of max-pooling operation using pool size [1 1 1] and stride [2 2] [Color figure can be viewed at wileyonlinelibrary.com]

TABLE 2 Proposed Layers detailed of 3D CNN architecture

Layer	Brief description
Input layer	32 × 32 × 3 with “zero center” normalization
Convolution 1	64 3 × 3 convolutions with stride [1 1] and padding [1 1 1]
ReLU activation	
Max Pooling 1	2 × 2 maxpool with stride [1 1] and padding [0 0 0]
Convolution 2	64 3 × 3 convolutions with stride [1 1] and padding [1 1 1]
ReLU activation	
Convolution 3	64 3 × 3 convolutions with stride [1 1] and padding [1 1 1]
ReLU activation	
Max Pool 2	2 × 2 maxpool with stride [2 2] and padding [0 0 0]
Transpose convolution	64 4 × 4 transposed convolutions with stride [2 2] and output cropping [1 1]
Convolution	2 1 × 1 convolution with stride [1 1] and padding [0 0 0]
Softmax layer	
Pixel classification layer	Cross entropy loss

100 and total 500 iterations, respectively. Mathematically, the sigmoid function $\sigma(Z)$ is formulated as:

$$Z = \sum_{i=1}^n w_i \phi_i + \beta_i, \quad (6)$$

$$\sigma(Z) = \frac{1}{1 + e^{-Z}} \quad (7)$$

The trained CNN is saved as a new network and utilized for the testing process. The obtained results are further refined through morphological operations like filling and closing with the help of the structuring element which is 7. The results are shown in Figure 6. Moreover, few other segmented results using the proposed method are shown in Figure 7.

3.4 | Features representation using deep learning

In machine learning, deep learning has shown impressive performance. The intellectual foundation of deep learning is rooted in the neural network (NN). However, in deep learning, unlike NN, deep learning involves many hidden layers and neurons (Khan et al., 2019; Khan et al., 2019; Saba, 2020). Data in deep learning are passed to the first

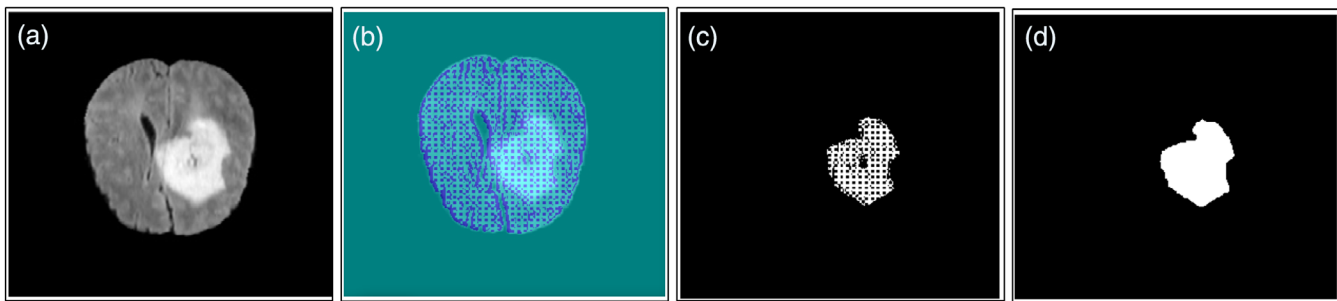
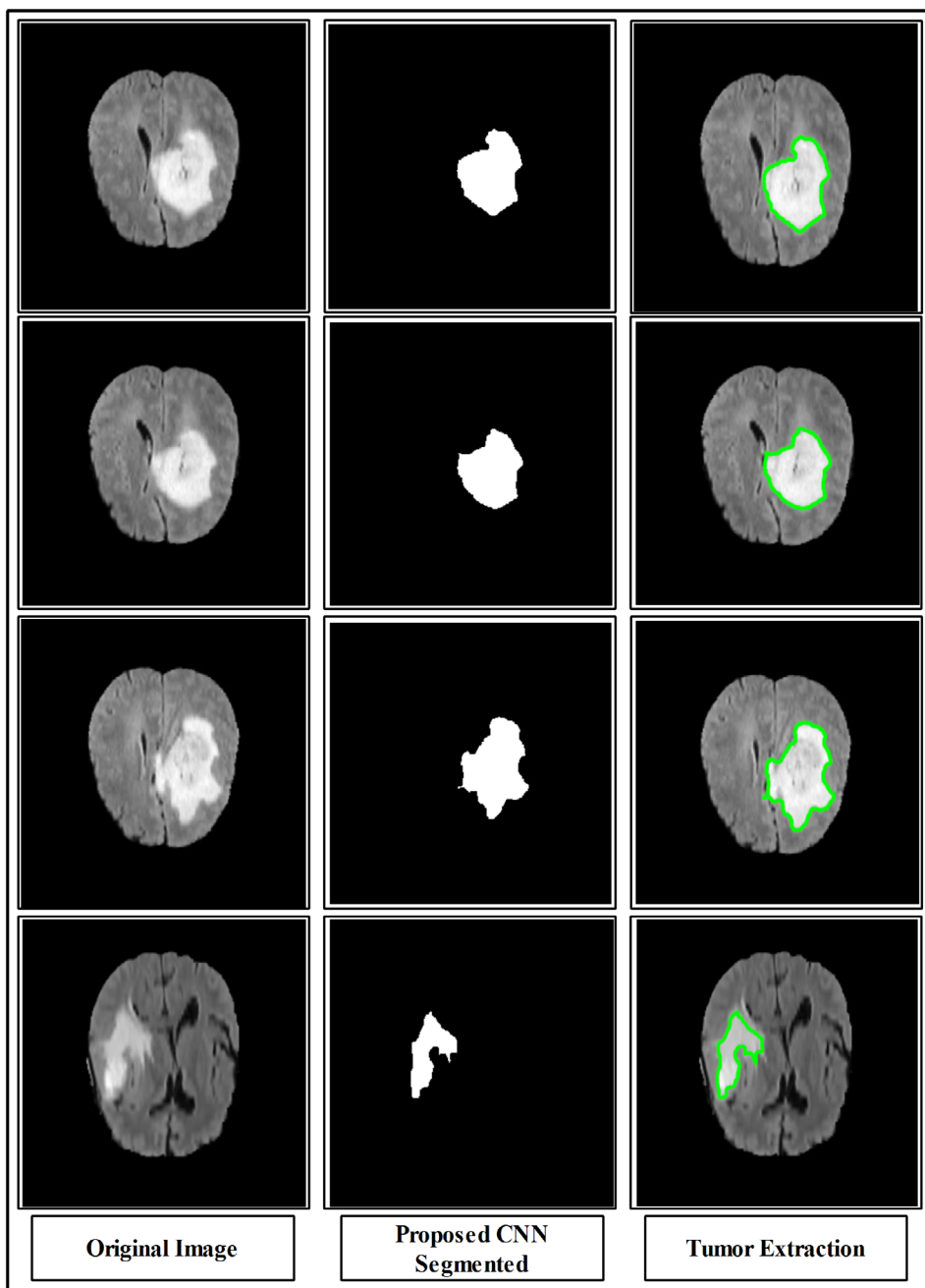


FIGURE 6 Proposed 3D CNN results using MRI scan. The original scan is illustrated in (a) while in (b) 3D CNN initial results, (c) 3D CNN tumor extracted results, and (d) results after refinement using morphological operations [Color figure can be viewed at wileyonlinelibrary.com]

FIGURE 7 Brain tumor derived results using proposed architecture
[Color figure can be viewed at wileyonlinelibrary.com]



layer to successive layer where between these two-layer several hidden layers are involved. As a result, high-level features are obtained for further classification. In medical imaging, the use of deep learning could help the practitioner for automatic classification of different problems like brain tumor grade, skin lesion, and so on (Javed, Saba, Shafry, & Rahim, 2020). Through deep learning, the automatic features are computed against each image that is much stronger than handcrafted features (Saba, Mohamed, et al., 2020).

CNN is a key technique of deep learning for automated feature extraction. A simple CNN model involves several numbers of layers such as convolution, ReLU, Pooling, Normalization, and Fully Connection. However, to train a new model from scratch require many resources like huge dataset, computational resources, and few others, therefore in this work, we utilized a pretrained model name VGG19 and trained on BraTS datasets with the help of transfer learning (Jaworek-Korjakowska, Kleczek, & Gorgon, 2019). A total of 143 M parameters are incorporated in this model used for the model learning on the ImageNet dataset. This dataset includes 1.2 M images of 1,000 different object categories. The internal architecture of this model includes 19 learnable layers including convolution, dropout, ReLU, and FC. From these layers, we only utilized the FC layer for training a new model on brain images and extract features. As we have multiple tumor classes, therefore a categorical loss function name cross-entropy is utilized. Mathematically, it is defined as:

$$\text{Loss} = - \sum_i^C t_i \log(f(s)_i) \quad (8)$$

$$f(s)_i = \frac{e^{s_i}}{\sum_j^C e^{s_j}} \quad (9)$$

where s_i is a standard softmax formulation, C denotes the number of tumor classes that are 4 in this work, and t depicts the class labels. The cross-entropy is applied to the FC layer and returned a feature vector of dimension $N \times 1,000$. However, due to error in 3D CN segmentation, a few features are not relevant therefore it is essential to remove these through a selection approach name correlation-based along with FNN (CbFNN).

The CbFNN is utilized to select the best feature set based on the correlation importance score. This method calculates the importance score for each feature. This importance score represents the importance of features and defined as follows (Mursalin, Zhang, Chen, & Chawla, 2017).

$$iS_{fs} = \frac{xC_{rf}}{\sqrt{x+x(x-1)C_{ff}}} \quad (10)$$

where iS_{fs} represents the importance score for the feature subset fs , C_{rf} is the correlation of response-feature, and C_{ff} is the feature-feature correlation. The most appropriate features are selected using importance score and neglect the irrelevant features to decrease the classification error. This method distinct the numeric features and

evaluates the relationship using symmetrical uncertainty. Entropy is utilized to find the degradation in features. The entropy and conditional entropy of the two random discrete variables M and N are described as:

$$E(N) = - \sum_{n \in N} p(n) \log p(n) \quad (11)$$

$$E(N|M) = - \sum_{m \in M} p(m) \sum_{n \in N} p(n|m) \log p(n|m) \quad (12)$$

Entropy and information gain estimate the importance of each feature for the classification. The information gain (IG) can be mathematically described as:

$$\varphi = E(N) - E(N|M) = E(N) + E(M) - E(M, N) \quad (13)$$

As information gain is influenced by the lower entropy features, to normalize the values symmetric uncertainty is utilized as described below:

$$\mu = 2.0 \times \left[\frac{\varphi}{E(N) + E(M)} \right] \quad (14)$$

The CbFNN calculates the correlation between the features and the response variable. The optimal features subset is obtained by utilizing a greedy search algorithm based on correlation values. These obtained values are put to FNN for validation up to 10 times. We set a check that if the validation accuracy is changed then again select features. This process continued up to 10 times iteration. The FNN utilized in this work as a fitness function to test the accuracy of the selected features. Mathematically, FNN formulated as follows:

$$\eta_j^l = \sum_{i=1}^{n_l-1} (w_{ij}^{l-1} y_i^{l-1} + \beta_j^l) \quad (15)$$

$$y_j^l = f(\eta_j^l) \quad (16)$$

4 | EXPERIMENTAL RESULTS AND EVALUATION

The proposed 3D CNN segmentation and tumor type classification results are presented in this section with detailed numerical and visual plots. As mentioned in Section 4.1, three BraTS datasets are utilized for validation such as 2015, 2017, and 2018, respectively. The FNN is utilized as a key classifier in this work while the few other classifiers such as Discriminant Analysis (LDA), K-Nearest Neighbor (KNN), Decision Trees (DT), and SVM are used for comparison. Various parameters are utilized for validation such as accuracy, error rate, and time.

Further, the mini-batch accuracy is also computed for segmentation performance. The detailed results are given below.

4.1 | Segmentation results and datasets

Two dataset names BraTS2015 and BraTS2018 are utilized in this work for validation of proposed 3D CNN architecture for tumor segmentation. For this purpose, several ratios are defined for training and testing of the proposed architecture as presented in Tables 3 and 4. In Table 3, the results of BraTS2015 dataset are presented for several ratios. For each ratio, the number of epochs, iterations, elapsed time, accuracy, MBL, and BLR are computed. The maximum attained mini-batch accuracy (MBtA) is 95.53% on BraTS2015 dataset where MBL is 0.0381. The minimum achieved MBtA is 92.51% on this dataset where the MBL is 0.0890 on ratio 10:90. On ratio (50:50), the attained MBtA is 94.99% along with reported MBL is 0.0301. These results are noted after 100 epochs and 500 iterations while the execution time of each selected ratio is noted and presented in this table. Further, the MBtA on all selected ratios is plotted in Figure 8 which shows the change in accuracy after change in training/testing ratio.

In Table 4, the results of BraTS 2018 dataset are presented for several ratios such as (80:20), (60:40), (50:50), and many more. For each ratio, the number of epochs, iterations, elapsed time, accuracy, MBL, and BLR are computed. The maximum attained mini-batch accuracy (MBtA) on this dataset is 95.44% on the ratio (80:20) where MBL is 0.0431. The minimum achieved MBtA is 93.18% on this dataset where the MBL is 0.0594 on ratio 60:40. On ratio (50:50), the attained MBtA is 95.34% along with reported MBL is 0.0586. These results are noted after 100 epochs and 500 iterations while the execution time of each selected ratio is noted and presented in this table. In the end, the attained MBtA on all selected ratios is also plotted in Figure 9 which confirms the change in accuracy after variation of selected ratios of training and testing. Overall proposed 3D CNN segmentation architecture outperforms on selected datasets which could be further visualized through results illustrated in Figure 10. In this

figure, the results of each image are compared with their ground-truth images.

4.2 | Classification results

The proposed architecture classification results are presented in this section. As shown in Figure 3, that features are extracted from the pretrained CNN model and later select the best of them using correlation along with the neural network. All the results are computed in the ratio (60:40) along with K-Fold is 10. Results are computed in two different ways—(a) original images are feed to pretrained model and select best features for final classification and (b) the proposed 3D CNN-based segmented images are passed to pretrained model and select best features. The results of BraTS 2015 dataset are presented in Table 5. In this table, it could be observed that the FNN achieves the highest accuracy of 97.36% on original images while the error rate and computational time are 2.6% and 106.309 (s), respectively. On the other hand, the accuracy of 98.32% is achieved on segmented images while error rate and computational time are 1.68% and 259.926 (s), respectively. Further, the results are also obtained on few other classifiers such as SVM, W-KNN, ES-KNN, LR, F-Tree, and Bagged-tree and achieved an accuracy of 95.29, 93.60, 89.94, 91.25, 84.92, and 88.92% for original images while for segmented images, the accuracy of 95.98, 94.21, 90.96, 93.36, 87.64, and 89.46%, respectively. The performance achieved on FNN is also validated through a confusion matrix, given in Figure 11. From the results, it is clear that the proposed method on FNN gives better results.

The results of BraTS 2017 dataset are presented in Table 6. In this table, it could be observed that the FNN achieves the highest accuracy of 94.96% on original images while the error rate and computational time are 5.04% and 116.420 (s), respectively. On the other hand, the accuracy of 96.97% is achieved on segmented images while error rate and computational time are 3.03% and 204.621 (s), respectively. Further, results are also obtained on few other classifiers such as SVM, W-KNN, ES-KNN, LR, F-Tree, and Bagged-tree and attained

TABLE 3 Proposed 3D CNN-based segmentation accuracy on BraTS2015 dataset using different training/testing ratio

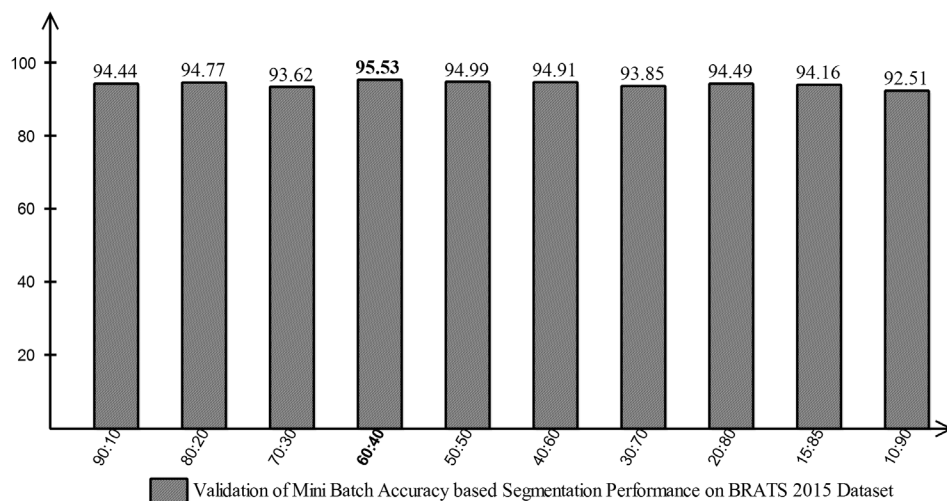
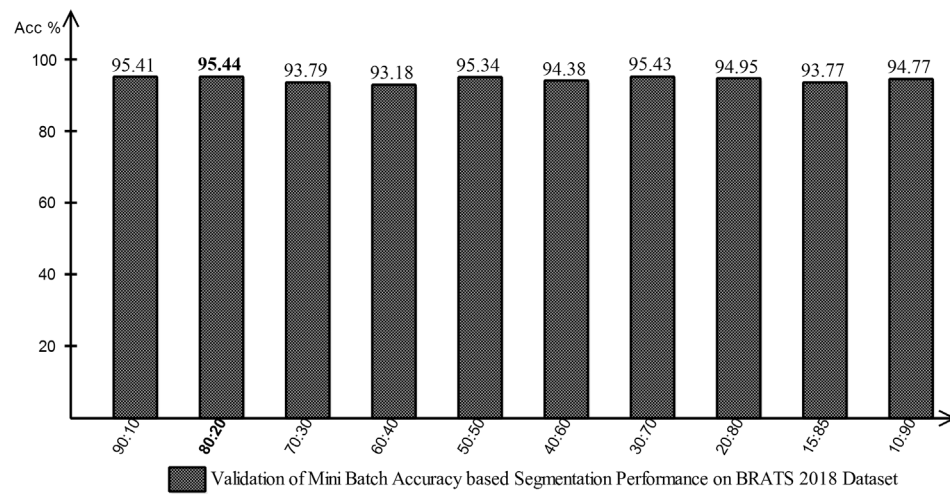
Ratio	Epochs	Iterations	Time elapsed	Mini-batch accuracy (%)	Mini-batch loss (MBL)	Base learning rate (BLR)
90:10	100	500	00:27:40	94.44	0.0434	0.0010
80:20	100	500	00:20:47	94.77	0.0383	0.0010
70:30	100	500	00:31:54	93.62	0.0669	0.0010
60:40	100	500	00:37:11	95.53	0.0381	0.0010
50:50	100	500	00:30:24	94.99	0.0301	0.0010
40:60	100	500	00:21:49	94.91	0.0477	0.0010
30:70	100	500	00:26:12	93.85	0.0799	0.0010
20:80	100	500	00:30:14	94.49	0.0600	0.0010
15:85	100	500	00:27:16	94.16	0.0571	0.0010
10:90	100	500	00:28:10	92.51	0.0890	0.0010

The bold values are showing best results achieved.

TABLE 4 Proposed 3D CNN-based segmentation accuracy on BraTS2018 dataset using different training/testing ratio

Ratio	Epochs	Iterations	Time elapsed	Mini-batch accuracy (%)	Mini-batch loss	Base learning rate
90:10	100	500	00:26:19	95.41	0.0369	0.0010
80:20	100	500	00:22:41	95.44	0.0431	0.0010
70:30	100	500	00:39:14	93.79	0.0541	0.0010
60:40	100	500	00:27:11	93.18	0.0594	0.0010
50:50	100	500	00:34:28	95.34	0.0586	0.0010
40:60	100	500	00:28:29	94.38	0.0696	0.0010
30:70	100	500	00:36:22	95.43	0.0365	0.0010
20:80	100	500	00:20:34	94.95	0.0377	0.0010
15:85	100	500	00:27:19	93.77	0.0499	0.0010
10:90	100	500	00:38:16	94.77	0.0549	0.0010

The bold values are showing best results achieved.

**FIGURE 8** Illustration of mini-batch accuracy on different training and testing ratios**FIGURE 9** Illustration of mini-batch accuracy on different training and testing ratios

an accuracy of 92.42, 92.66, 91.10, 92.54, 88.44, and 81.93% for original images while attained accuracy on segmented images is 95.59, 94.59, 91.94, 93.90, 88.90, and 83.56%, respectively. The performance achieved on FNN is also validated through a confusion matrix,

given in Figure 12. From the results, it is clear that the proposed method on FNN gives improved performance.

The results of BraTS 2018 dataset are presented in Table 7. In this table, it can be observed that the FNN achieves the highest

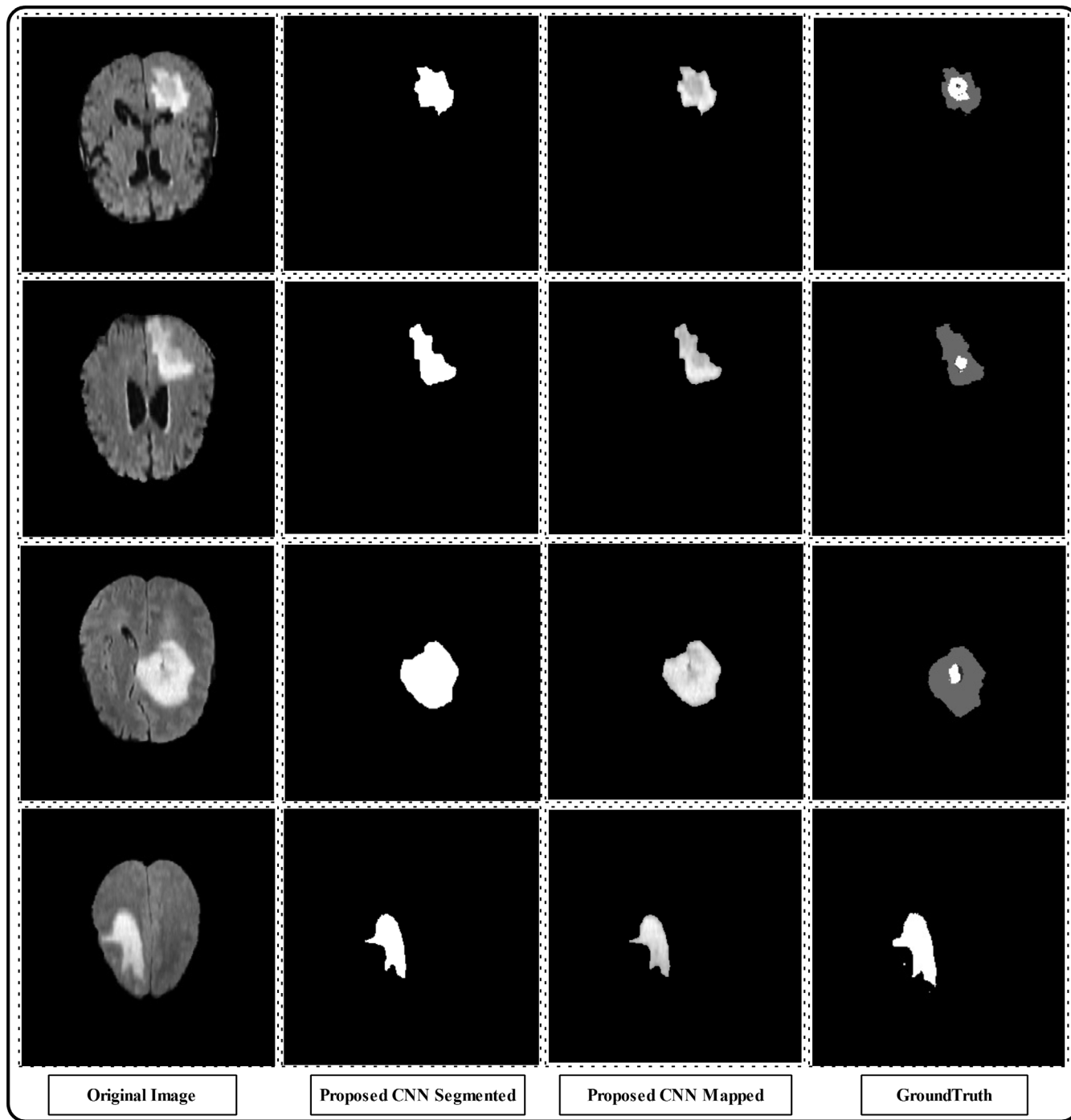


FIGURE 10 Proposed 3D CNN segmentation results for brain tumor extraction

accuracy of 90.42% on original images while the error rate and computational time are 9.58% and 117.428 (s), respectively. On the other hand, the accuracy of 92.67% is achieved on segmented images while error rate and computational time are 7.33% and 266.677 (s), respectively. Further, results are also obtained on few other classifiers such as SVM, W-KNN, ES-KNN, LR, F-Tree, and Bagged-tree and attained an accuracy of 87.59, 87.66, 89.42, 80.46, 85.16, and 85.05% for original images while attained accuracy on segmented images is 89.36, 88.03, 89.98, 82.62, 87.39, and 86.17%, respectively. The

performance achieved on FNN is also validated through a confusion matrix, given in Figure 13. From the results, it is clear that the proposed method on FNN yields better performance.

4.3 | Analysis and discussion

In this section, a detailed analysis of the proposed method is described. As shown in Figure 3, the proposed method consists of two key steps:

Method	Original images	3D CNN segmented	Measures		
			Accuracy (%)	Error (%)	Time (s)
FNN	✓		97.36	2.64	106.39
		✓	98.32	1.68	259.926
SVM	✓		95.29	4.71	97.624
		✓	95.98	4.02	197.690
W-KNN	✓		9,360	6.40	150.406
		✓	94.21	5.79	270.929
ES-KNN	✓		89.94	10.06	169.936
		✓	90.96	9.04	297.606
LR	✓		91.25	8.75	125.421
		✓	93.36	6.64	183.694
F-tree	✓		84.92	15.08	93.401
		✓	87.64	12.36	116.436
Baggage tree	✓		88.92	11.08	197.234
		✓	89.46	1,054	295.549

The bold values are showing best results achieved.

TABLE 5 Proposed tumor type classification results using BraTS2015 dataset

Tumor Type	Tumor type			
	Flair	T1CE	T1	T2
Flair	96.4%	2%	1%	<1%
T1CE	<1%	99.3%	<1%	
T1		1%	98.2%	<1%
T2	<1%	2%	2%	95.4%

Tumor Type	Tumor type			
	Flair	T1CE	T1	T2
Flair	97.1%	2%	<1%	<1%
T1CE	<1%	99%	<1%	
T1	<1%	1%	98.4%	<1%
T2		1%	<1%	98.6%

FIGURE 11 Confusion matrix of BraTS2015 dataset where (a) represents a confusion matrix of original images based classification while (b) depicts the 3D CNN based extracted tumor for classification [Color figure can be viewed at wileyonlinelibrary.com]

Method	Original images	3D CNN segmented	Measures		
			Accuracy (%)	Error (%)	Time (s)
FNN	✓		94.96	5.04	116.420
		✓	96.97	3.03	204.621
SVM	✓		94.42	5.58	104.826
		✓	95.59	4.41	184.542
W-KNN	✓		92.69	7.31	129.509
		✓	94.59	5.41	214.428
ES-KNN	✓		91.10	8.90	147.460
		✓	91.94	8.06	217.519
LR	✓		92.54	7.46	114.432
		✓	93.90	6.10	241.594
F-tree	✓		88.44	11.56	136.446
		✓	88.90	11.10	269.101
Baggage tree	✓		81.93	18.07	151.596
		✓	83.56	16.44	257.667

The bold values are showing best results achieved.

TABLE 6 Proposed tumor type classification results using BraTS2017 dataset

Tumor Type	Tumor type			
	Flair	T1CE	T1	T2
Flair	93.68%	4%	2%	<1%
T1CE	4%	92.42%	<1%	3%
T1	3%		95.0%	2%
T2	<1%		1%	98.6%

Tumor Type	Tumor type			
	Flair	T1CE	T1	T2
Flair	95%	3%		2%
T1CE	1%	97%	2%	
T1	2%	<1%	97.6%	
T2		<1	1%	98.2%

FIGURE 12 Confusion matrix of BraTS2017 dataset where (a) represents a confusion matrix of original images based classification while (b) depicts the 3D CNN based extracted tumor for classification [Color figure can be viewed at wileyonlinelibrary.com]

TABLE 7 Proposed tumor type classification results using BraTS2018 dataset

Method	Original images	3D CNN segmented	Measures		
			Accuracy	Error	Time
FNN	✓		90.42	9.58	117.428
		✓	92.67	7.33	266.677
SVM	✓		87.59	12.41	141.596
		✓	89.36	10.64	271.400
W-KNN	✓		87.66	12.34	104.639
		✓	88.03	11.97	198.089
ES-KNN	✓		89.42	10.58	136.634
		✓	89.98	10.02	211.506
LR	✓		80.46	19.54	121.607
		✓	82.62	17.38	204.607
F-tree	✓		85.16	14.84	116.554
		✓	87.39	12.61	241.592
Baggage tree	✓		85.00	15.00	126.448
		✓	86.17	13.83	276.637

The bold values are showing best results achieved.

Tumor Type	Tumor type			
	Flair	T1CE	T1	T2
Flair	89.8%	5%	5%	2%
T1CE	<1%	93.4%	3%	3%
T1	1%	4%	91.0%	4%
T2	<1%	6%	6%	87.4%

Tumor Type	Tumor type			
	Flair	T1CE	T1	T2
Flair	90.4%	4%	5%	<1%
T1CE	<1%	92.8%	3%	4%
T1	3%	4%	92.0%	1%
T2	<1%	2%	2%	95.6%

FIGURE 13 Confusion matrix of BraTS2018 dataset where (a) represents a confusion matrix of original images based classification while (b) depicts the 3D CNN based extracted tumor for classification [Color figure can be viewed at wileyonlinelibrary.com]

Tumor extraction and Tumor type classification. The architecture of 3D CNN for tumor extraction is shown in Figure 4 and its parameter detail is given in Table 2. The results of this architecture are presented in

Tables 3 and 4 for selected datasets BraTS 2015 and BraTS 2018. On BraTS 2015, the maximum achieved accuracy is 95.53% on the ratio (60:40) while the MBL is 0.0381. For the BraTS 2018 dataset, the

TABLE 8 Comparison with existing techniques on BraTS benchmark datasets

Method	Classifier	Dataset	Accuracy (%)
Khan et al. (2020)	CNN	BraTS 2015	97.8 (accuracy)
		BraTS 2017	96.9 (accuracy)
		BraTS 2018	92.5 (accuracy)
Saba, Haseeb, Ahmed, and Rehman (2020)	CNN	BraTS 2015	98.78(accuracy)
		BraTS 2016	99.63(accuracy)
		BraTS 2017	99.67(accuracy)
Sharif et al. (2020)	CNN	BraTS 2015	97.80 (accuracy)
		BraTS 2017	96.90 (accuracy)
		BraTS 2018	92.50 (accuracy)
Iqbal et al. (2019)	CNN	BraTS 2015	82.29 (accuracy)
Sajjad et al. (2019)	CNN	BraTS 2015	94.58 (accuracy)
Wasule and Sonar (2017)	SVM and KNN	BraTS 2012	85 (accuracy) 72.50 (accuracy)
Vaishnavee and Amshakala (2015)	Proximal Support vector machines (PSVM)	BraTS 2015	92 (accuracy) 94 (recall) 93 (precision)
Proposed	3D CNN	BraTS 2015	98.32 (accuracy)
		BraTS 2017	96.97 (accuracy)
		BraTS 2018	92.67 (accuracy)

maximum attained an accuracy of 95.44% on the ratio (80:20). The segmentation accuracy of both datasets is also plotted in Figures 8 and 9. Further, the visual results are shown in Figures 6, 7, and 10. From the results, it could be observed that the proposed segmentation design significantly works on low contrast tumor regions.

As presented in Figure 3, the classification process is performed using the pretrained model. The selected pretrained model is trained through transfer learning on the BraTS datasets of ratio (60:40) and extract features separately. However, due to loss in the segmentation process, a few irrelevant features have involved that cause a problem in the classification process. Therefore, a selection approach is proposed and selects the best features. These features are classified through FNN. The results are presented on different datasets are given in Tables 5–7 that further verified through Figures 11–13. The results show that the accuracy of the proposed selection method is improved after 3D CNN segmentation compared to original images. However, the computation time of the segmented approach increases almost double as compared to original images when it provides to pretrained model for training. Furthermore, it is also observed that the selection process improves the accuracy of the selected datasets.

A comprehensive comparison is also conducted at the end of the validation of the proposed method. A brief comparison is conducted in Table 8. In this table, it is described that Sharif et al. (2020) utilized three BraTS datasets name 2015, 2017, and 2018 and attained an accuracy of 97.8, 96.9, and 92.5%.

Recently, Khan et al. (2020) employed two pretrained CNN models, VGG16 and VGG19, for feature extraction. The selected features were fed to ELM for brain tumor classification and achieved 97.8, 96.9, 92.5% on BraTS 2015, BraTS 2017, BraTS 2018 datasets, respectively. Wasule

and Sonar (2017) used texture features for brain tumor classification using supervised SVM and KNN algorithm. They reported accuracy 96 and 86% for SVM and KNN, respectively, for clinical database and 85 and 72.50% for SVM and KNN, respectively, for Brats 2012 database. Vaishnavee and Amshakala (2015) employed proximal support vector machines (PSVM) for automatic detection of tumor from MRI brain images. They reported 92% (Accuracy), 94% (Recall), 93% (Precision) on BraTS 2015.

While, the proposed method validated on the same datasets and attained 98.32, 96.97, and 92.67% accuracy. The results exhibit that the proposed method reported improved performance as compared to existing methods.

5 | CONCLUSION AND FUTURE WORK

3D DNN-based architecture is proposed in this work for brain tumor extraction and tumor type classification. The tumor is extracted from MRI scans using proposed 3D CNN architecture while the classification process is done by transfer learning. A pretrained CNN model VGG19 is employed for feature extraction and later selects the best feature by the proposed CbFNN approach. The selected features are validated through FNN. Three BraTS datasets such as 2015, 2017, and 2018 are utilized for validation and achieved satisfactory performance. From results, we conclude that the proposed 3D CNN model segment the tumor with high precision and less error rate. Further, the proposed architecture correctly segments the tumor from low contrast MRI scans. Besides, the classification accuracy of tumor type's classification is increased when a pretrained model is trained by extracted tumor images but on the other hand, the classification time

is increased as compared to trained pretrained model by original MRI scans. In the future, a deep reinforcement learning model will be implemented for brain tumor classification.

ACKNOWLEDGMENTS

This work was funded by the research project [Brain Tumor Detection and Classification using 3D CNN and Feature Selection Architecture]; Prince Sultan University; Saudi Arabia [SEED-CCIS-2020[30]]. The authors are thankful for the support.

ORCID

Amjad Rehman  <https://orcid.org/0000-0002-3817-2655>

Muhammad Attique Khan  <https://orcid.org/0000-0002-6347-4890>

Tanzila Saba  <https://orcid.org/0000-0003-3138-3801>

Zahid Mehmood  <https://orcid.org/0000-0003-4888-2594>

Usman Tariq  <https://orcid.org/0000-0001-7672-1187>

REFERENCES

- Abbas, N., Saba, T., Rehman, A., Mehmood, Z., Kolivand, H., Uddin, M., & Anjum, A. (2018). Plasmodium life cycle stage classification based quantification of malaria parasitaemia in thin blood smears. *Microscopy Research and Technique*, 82(3), 283–295. <https://doi.org/10.1002/jemt.23170>
- Abbas, N., Saba, T., Mohamad, D., Rehman, A., Almazyad, A. S., & Al-Ghamdi, J. S. (2018). Machine aided malaria parasitemia detection in Giemsa-stained thin blood smears. *Neural Computing and Applications*, 29(3), 803–818. <https://doi.org/10.1007/s00521-016-2474-6>
- Abbas, A., Saba, T., Rehman, A., Mehmood, Z., Javaid, N., Tahir, M., ... Shah, R. (2019). Plasmodium species aware based quantification of malaria, parasitemia in light microscopy thin blood smear. *Microscopy Research and Technique*, 82(7), 1198–1214. <https://doi.org/10.1002/jemt.23269>
- Abbas, N., Saba, T., Mehmood, Z., Rehman, A., Islam, N., & Ahmed, K. T. (2019). An automated nuclei segmentation of leukocytes from microscopic digital images. *Pakistan Journal of Pharmaceutical Sciences*, 32(5), 2123–2138.
- Al-Ameen, Z., Sulong, G., Rehman, A., Al-Dhelaan, A., Saba, T., & Al-Rodhaan, M. (2015). An innovative technique for contrast enhancement of computed tomography images using normalized gamma-corrected contrast-limited adaptive histogram equalization. *EURASIP Journal on Advances in Signal Processing*, 2015, 32. <https://doi.org/10.1186/s13634-015-0214-1>
- Afza, F., Khan, M. A., Sharif, M., & Rehman, A. (2019). Microscopic skin laceration segmentation and classification: A framework of statistical normal distribution and optimal feature selection. *Microscopy Research and Technique*, 82(9), 1471–1488.
- Amin, J., Sharif, M., Raza, M., Saba, T., Sial, R., & Shad, S. A. (2019). Brain tumor detection: A long short-term memory (LSTM)-based learning model. *Neural Computing and Applications*, 1–9.
- Amin, J., Sharif, M., Yasmin, M. T. S., & Raza, M. (2019). Use of machine intelligence to conduct analysis of human brain data for detection of abnormalities in its cognitive functions. *Multimedia Tools and Applications* (2019, 79, 10955–10973. <https://doi.org/10.1007/s11042-019-7324-y>
- Arunkumar, N., Mohammed, M. A., Mostafa, S. A., Ibrahim, D. A., Rodrigues, J. J., & de Albuquerque, V. H. C. (2020). Fully automatic model-based segmentation and classification approach for MRI brain tumor using artificial neural networks. *Concurrency and Computation: Practice and Experience*, 32(1), e4962.
- Banerjee, S., Mitra, S., & Shankar, B. U. (2018). Automated 3D segmentation of brain tumor using visual saliency. *Information Sciences*, 424, 337–353.
- Ejaz, K., Rahim, M. S. M., Bajwa, U. I., Chaudhry, H., Rehman, A., & Ejaz, F. (2020). Hybrid segmentation method with confidence region detection for tumor identification. *IEEE Access*. <https://doi.org/10.1109/ACCESS.2020.3016627>
- Ejaz, K., Rahim, M. S. M., Rehman, A., Chaudhry, H., Saba, T., Ejaz, A., & Ej, C. F. (2018). Segmentation method for pathological brain tumor and accurate detection using MRI. *International Journal of Advanced Computer Science and Applications*, 9(8), 394–401.
- Fahad, H. M., Khan, M. U. G., Saba, T., Rehman, A., & Iqbal, S. (2018). Microscopic abnormality classification of cardiac murmurs using ANFIS and HMM. *Microscopy Research and Technique*, 81(5), 449–457. <https://doi.org/10.1002/jemt.22998>
- Grade, M., Tamames, J. H., Pizzini, F., Achten, E., Golay, X., & Smits, M. (2015). A neuroradiologist's guide to arterial spin labeling MRI in clinical practice. *Neuroradiology*, 57(12), 1181–1202.
- Husham, A., Alkawaz, M. H., Saba, T., Rehman, A., & Alghamdi, J. S. (2016). Automated nuclei segmentation of malignant using level sets. *Microscopy Research and Technique*, 79(10), 993–997. <https://doi.org/10.1002/jemt.22733>
- Iftikhar, S., Fatima, K., Rehman, A., Almazyad, A. S., & Saba, T. (2017). An evolution based hybrid approach for heart diseases classification and associated risk factors identification. *Biomedical Research*, 28(8), 3451–3455.
- Iqbal, S., Khan, M. U. G., Saba, T., & Rehman, A. (2017). Computer assisted brain tumor type discrimination using magnetic resonance imaging features. *Biomedical Engineering Letters*, 8(1), 5–28. <https://doi.org/10.1007/s13534-017-0050-3>
- Iqbal, S., Ghani, M. U., Saba, T., & Rehman, A. (2018). Brain tumor segmentation in multi-spectral MRI using convolutional neural networks (CNN). *Microscopy Research and Technique*, 81(4), 419–427. <https://doi.org/10.1002/jemt.22994>
- Iqbal, S., Ghani Khan, M. U., Saba, T., Mehmood, Z., Javaid, N., Rehman, A., & Abbasi, R. (2019). Deep learning model integrating features and novel classifiers fusion for brain tumor segmentation. *Microscopy Research and Technique*, 82(8), 1302–1315. <https://doi.org/10.1002/jemt.23281>
- Jadooki, S., Mohamad, D., Saba, T., Almazyad, A. S., & Rehman, A. (2017). Fused features mining for depth-based hand gesture recognition to classify blind human communication. *Neural Computing and Applications*, 28(11), 3285–3294. <https://doi.org/10.1007/s00521-016-2244-5>
- Javed, R., Rahim, M. S. M., Saba, T., & Rashid, M. (2019). Region-based active contour JSEG fusion technique for skin lesion segmentation from dermoscopic images. *Biomedical Research*, 30(6), 1–10.
- Javed, R., Rahim, M. S. M., & Saba, T. (2019). An improved framework by mapping salient features for skin lesion detection and classification using the optimized hybrid features. *International Journal of Advanced Trends in Computer Science and Engineering*, 8(1), 95–101.
- Javed, R., Rahim, M. S. M., Saba, T., & Rehman, A. (2020). A comparative study of features selection for skin lesion detection from dermoscopic images. *Network Modeling Analysis in Health Informatics and Bioinformatics*, 9(1), 4.
- Javed, R., Saba, T., Shafry, M., & Rahim, M. (2020). An intelligent saliency segmentation technique and classification of low contrast skin lesion dermoscopic images based on histogram decision. In 2019 12th International Conference on Developments in eSystems Engineering (DeSE) (pp. 164–169).
- Jamal, A., Hazim Alkawaz, M., Rehman, A., & Saba, T. (2017). Retinal imaging analysis based on vessel detection. *Microscopy Research and Technique*, 80(17), 799–811. <https://doi.org/10.1002/jemt>
- Jaworek-Korjakowska, J., Kleczek, P., & Gorgon, M. (2019). Melanoma thickness prediction based on convolutional neural network with VGG-19 model transfer learning. Paper presented at the Proceedings of the IEEE Conference on Computer Vision and Pattern Recognition Workshops.
- Khan, M. A., Akram, T., Sharif, M., Awais, M., Javed, K., Ali, H., & Saba, T. (2018). CCDF: Automatic system for segmentation and recognition of

- fruit crops diseases based on correlation coefficient and deep CNN features. *Computers and Electronics in Agriculture*, 155, 220–236.
- Khan, M. A., Lali, I. U., Rehman, A., Ishaq, M., Sharif, M., Saba, T., ... Akram, T. (2019). Brain tumor detection and classification: A framework of marker-based watershed algorithm and multilevel priority features selection. *Microscopy Research and Technique*, 82(6), 909–922.
- Khan, M. A., Sharif, M. I., Raza, M., Anjum, A., Saba, T., & Shad, S. A. (2019). Skin lesion segmentation and classification: A unified framework of deep neural network features fusion and selection. *Expert Systems*, e12497.
- Khan, M. A., Akram, T., Sharif, M., Saba, T., Javed, K., Lali, I. U., ... Rehman, A. (2019). Construction of saliency map and hybrid set of features for efficient segmentation and classification of skin lesion. *Microscopy Research and Technique*, 82, 741–763. <http://doi.org/10.1002/jemt.23220>
- Khan, M. A., Ashraf, I., Alhaisoni, M., Damaševičius, R., Scherer, R., Rehman, A., & Bukhari, S. A. C. (2020). Multimodal brain tumor classification using deep learning and robust feature selection: A machine learning application for radiologists. *Diagnostics*, 10, 565.
- Mittal, A., Kumar, D., Mittal, M., Saba, T., Abunadi, I., Rehman, A., & Roy, S. (2020). Detecting pneumonia using convolutions and dynamic capsule routing for chest X-ray images. *Sensors*, 20(4), 1068.
- Mughal, B., Muhammad, N., Sharif, M., Rehman, A., & Saba, T. (2018). Removal of pectoral muscle based on topographic map and shape-shifting silhouette. *BMC Cancer*, 18, 778. <https://doi.org/10.1186/s12885-018-4638-5>
- Mughal, B., Muhammad, N., Sharif, M., Saba, T., & Rehman, A. (2017). Extraction of breast border and removal of pectoral muscle in wavelet domain. *Biomedical Research*, 28(11), 5041–5043.
- Mughal, B., Sharif, M., Muhammad, N., & Saba, T. (2017). A novel classification scheme to decline the mortality rate among women due to breast tumor. *Microscopy Research and Technique*, 81(2), 171–180. <https://doi.org/10.1002/jemt.22961>
- Marie-Sainte, S. L., Saba, T., Alsaleh, D., Alotaibi, A., & Bin, M. (2019). An improved strategy for predicting diagnosis, survivability, and recurrence of breast cancer. *Journal of Computational and Theoretical Nanoscience*, 16(9), 3705–3711.
- Mursalin, M., Zhang, Y., Chen, Y., & Chawla, N. V. J. N. (2017). Automated epileptic seizure detection using improved correlation-based feature selection with random forest classifier, 241, 204–214.
- Nanda, S. J., Gulati, I., Chauhan, R., Modi, R., & Dhaked, U. (2019). A K-means-galactic swarm optimization-based clustering algorithm with Otsu's entropy for brain tumor detection. *Applied Artificial Intelligence*, 33(2), 152–170.
- Nazir, M., Khan, M. A., Saba, T., & Rehman, A. (2019). Brain tumor detection from MRI images using multi-level wavelets. International Conference on Computer and Information Sciences (ICCIS).
- Norouzi, A., Rahim, M. S. M., Altameem, A., Saba, T., Rada, A. E., Rehman, A., & Uddin, M. (2014). Medical image segmentation methods, algorithms, and applications. *IETE Technical Review*, 31(3), 199–213. <https://doi.org/10.1080/02564602.2014.906861>
- NBTC. (2019). Quick brain tumor facts. Retrieved from <https://braintumor.org/brain-tumor-information/brain-tumor-facts/>
- Padlia, M., & Sharma, J. (2019). Fractional Sobel filter based brain tumor detection and segmentation using statistical features and SVM. *Nanoelectronics, circuits and communication systems* (pp. 161–175).
- Perveen, S., Shahbaz, M., Saba, T., Keshavjee, K., Rehman, A., & Guergachi, A. (2020). Handling irregularly sampled longitudinal data and prognostic modeling of diabetes using machine learning technique. *IEEE Access*, 8, 21875–21885.
- Rehman, A., Abbas, N., Saba, T., Rahman, S. I. U., Mehmood, Z., & Kolivand, H. (2018). Classification of acute lymphoblastic leukemia using deep learning. *Microscopy Research and Technique*, 81(11), 1310–1317.
- Rehman, A., Abbas, N., Saba, T., Mehmood, Z., Mahmood, T., & Ahmed, K. T. (2018). Microscopic malaria parasitemia diagnosis and grading on benchmark datasets. *Microscopic Research and Technique*, 81(9), 1042–1058. <https://doi.org/10.1002/jemt.23071>
- Rehman, A., Abbas, N., Saba, T., Mahmood, T., & Kolivand, H. (2018). Rouleaux red blood cells splitting in microscopic thin blood smear images via local maxima, circles drawing, and mapping with original RBCs. *Microscopic Research and Technique*, 81(7), 737–744. <https://doi.org/10.1002/jemt.23030>
- Rehman, A., Khan, M. A., Mehmood, Z., Saba, T., Sardaraz, M., & Rashid, M. (2020). Microscopic melanoma detection and classification: A framework of pixel-based fusion and multilevel features reduction. *Microscopy Research and Technique*, 83, 410–423.
- Ramzan, F., Khan, M. U. G., Iqbal, S., Saba, T., & Rehman, A. (2020). Volumetric segmentation of brain regions from MRI scans using 3D convolutional neural networks. *IEEE Access*, 8, 103697–103709.
- Ramzan, F., Khan, M. U. G., Rehmat, A., Iqbal, S., Saba, T., Rehman, A., & Mehmood, Z. (2020). A deep learning approach for automated diagnosis and multi-class classification of Alzheimer's disease stages using resting-state fMRI and residual neural networks. *Journal of Medical Systems*, 44(2), 37.
- Rahim, M. S. M., Norouzi, A., Rehman, A., & Saba, T. (2017). 3D bones segmentation based on CT images visualization. *Biomedical Research*, 28(8), 3641–3644.
- Rahim, M. S. M., Rehman, A., Kurniawan, F., & Saba, T. (2017). Ear biometrics for human classification based on region features mining. *Biomedical Research*, 28(10), 4660–4664.
- Saba, T., Mohamed, A. S., El-Affendi, M., Amin, J., & Sharif, M. (2020). Brain tumor detection using fusion of hand crafted and deep learning features. *Cognitive Systems Research*, 59, 221–230.
- Saba, T., Haseeb, K., Ahmed, I., & Rehman, A. (2020). Secure and energy-efficient framework using internet of medical things for e-healthcare. *Journal of Infection and Public Health*. <https://doi.org/10.1016/j.jiph.2020.06.027>
- Saba, T. (2020). Recent advancement in cancer detection using machine learning: Systematic survey of decades, comparisons and challenges. *Journal of Infection and Public Health*, 13(9), 1274–1289. <https://doi.org/10.1016/j.jiph.2020.06.033>
- Saba, T., Khan, M. A., Rehman, A., & Marie-Sainte, S. L. (2019). Region extraction and classification of skin cancer: A heterogeneous framework of deep CNN features fusion and reduction. *Journal of Medical Systems*, 43(9), 289.
- Saba, T., Sameh, A., Khan, F., Shad, S. A., & Sharif, M. (2019). Lung nodule detection based on ensemble of hand crafted and deep features. *Journal of Medical Systems*, 43(12), 332.
- Saba, T., Khan, S. U., Islam, N., Abbas, N., Rehman, A., Javaid, N., & Anjum, A. (2019). Cloud-based decision support system for the detection and classification of malignant cells in breast cancer using breast cytology images. *Microscopy Research and Technique*, 82(6), 775–785.
- Saba, T., Rehman, A., Mehmood, Z., Kolivand, H., & Sharif, M. (2018). Image enhancement and segmentation techniques for detection of knee joint diseases: A survey. *Current Medical Imaging Reviews*, 14(5), 704–715. <https://doi.org/10.2174/1573405613666170912164546>
- Saba, T., Bokhari, S. T. F., Sharif, M., Yasmin, M., & Raza, M. (2018). Fundus image classification methods for the detection of glaucoma: A review. *Microscopy Research and Technique*, 81, 1105–1121. <https://doi.org/10.1002/jemt.23094>
- Saba, T. (2017). Halal food identification with neural assisted enhanced RFID antenna. *Biomedical Research*, 28(18), 7760–7762.
- Sajid, S., Hussain, S., & Sarwar, A. (2019). Brain tumor detection and segmentation in MR images using deep learning. *Arabian Journal for Science and Engineering*, 44(11), 9249–9261.
- Sajjad, M., Khan, S., Muhammad, K., Wu, W., Ullah, A., & Baik, S. W. (2019). Multi-grade brain tumor classification using deep CNN with extensive data augmentation. *Journal of Computational Science*, 30, 174–182.
- Sharif, M. I., Li, J. P., Khan, M. A., & Saleem, M. A. (2020). Active deep neural network features selection for segmentation and recognition of brain tumors using MRI images. *Pattern Recognition Letters*, 129, 181–189.

- Tahir, B., Iqbal, S., Khan. M. U. G., Saba, T., Mehmood, Z., Anjum, A., Mahmood, T. (2019) Feature enhancement framework for brain tumor segmentation and classification, <https://doi.org/10.1002/jemt.23224>.
- Ullah, H., Saba, T., Islam, N., Abbas, N., Rehman, A., Mehmood, Z., & Anjum, A. (2019). An ensemble classification of exudates in color fundus images using an evolutionary algorithm based optimal features selection. *Microscopy Research and Technique*, 82(4), 361–372. <https://doi.org/10.1002/jemt.23178>
- Vaishnavi, K., & Amshakala, K. (2015). An automated MRI brain image segmentation and tumor detection using SOM-clustering and proximal support vector machine classifier. In: 2015 IEEE International Conference on Engineering and Technology (ICETECH). (pp. 1–6).
- Wasule, V., & Sonar, P. (2017). Classification of brain MRI using SVM and KNN classifier. In: Third International Conference on Sensing, Signal Processing and Security (ICSSS) (pp. 218–223).
- Yousaf, K., Mehmood, Z., Saba, T., Rehman, A., Munshi, A. M., Alharbey, R., & Rashid, M. (2019). Mobile-health applications for the efficient delivery of health care facility to people with dementia (PWD) and support to their carers: A survey. *BioMed Research International*, 2019, 1–26.

How to cite this article: Rehman A, Khan MA, Saba T, Mehmood Z, Tariq U, Ayesha N. Microscopic brain tumor detection and classification using 3D CNN and feature selection architecture. *Microsc Res Tech*. 2020;1–17. <https://doi.org/10.1002/jemt.23597>